ACS APPLIED MATERIALS & INTERFACES

Research Article

www.acsami.org

Screw Dislocations in Complex, Low Symmetry Oxides: Core Structures, Energetics, and Impact on Crystal Growth

Rouzbeh Shahsavari*[,†,‡,§] and Lu Chen[†]

[†]Department of Civil and Environmental Engineering, [‡]Department of Material Science and NanoEngineering, [§]Smalley Institute for Nanoscale Science and Technology, Rice University, Houston, Texas 77005, United States

Supporting Information

ABSTRACT: Determining the atomic structure and the influence of defects on properties of low symmetry oxides have long been an engineering pursuit. Here, we focus on five thermodynamically reversible monoclinic and orthorhombic polymorphs of dicalcium silicates (Ca_2SiO_3)—a key cement constituent—as a model system and use atomistic simulations to unravel the interplay between the screw dislocation core energies, nonplanar core structures, and Peierls stresses along different crystallographic planes. Among different polymorphs, we found that the α polymorphs (α-C_2S) has the largest Peierls stress, corresponding to the most brittle polymorph, which make it attractive for grinding processes. Interestingly, our analyses indicate that this polymorphs has the lowest dislocation core energy, making it ideal for reactivity and crystal growth. Generally, we identified the following order in terms of grinding efficiency based on screw dislocation analysis, α-C_2S > α_H-C_2S > α_L-C_2S > β-C_2S > γ-C_2S, and the following order in term of reactivity, α -C_2S > α_L-C_2S > γ-C_2S > α_H-C_2S > β-C_2S. This information, combined with other deformation-based mechanisms, such as twinning and edge dislocation, can provide crucial insights and guiding hypotheses for experimentalists to tune the cement grinding mechanisms and reactivity processes for an overall optimum solution with regard to both energy consumption and performance. Our findings significantly broaden the spectrum of strategies for leveraging both crystallographic directions and crystal symmetry to concurrently modulate mechanics and crystal growth processes within an identical chemical composition.

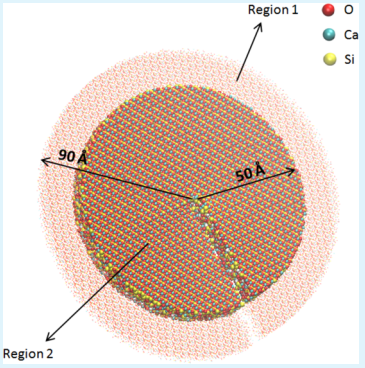

KEYWORDS: *dicalcium silicates (Ca_2SiO_3), atomistic simulation, screw dislocation, crystal defects, dislocation-mediated property, Peierls stress*

INTRODUCTION

Microscale defects such as stacking faults and dislocations, which form and propagate in crystals, significantly influence many chemical and physical properties of materials. For instance, crystal growth is generally controlled by a screw dislocation terminated at the surface.[1] Similarly, material plasticity and crack propagation are substantially influenced by dislocation core structure, dislocation-dislocation interactions, and dislocation motilities.[2] While dislocations have been widely observed and studied in metals[3−6] semiconductors[7−11] and some simple ceramics,[12−19] there have been few attempts in characterizing such defects in more complex compounds such as zeolites, forsterite (Mg_2SiO_4) and dicalcium silicates (Ca_2SiO_3).[20] The difficulty arises due to the heterogeneous nature, the complicated formatting components, and the packing arrangements of several atomic species, which often lead to low symmetry crystals.

There exist several experimental techniques such as surface and decoration methods, field ion microscopy, X-ray diffraction, high-resolution transmission electron microscopy (HRTEM), and Z-contrast imaging techniques to study dislocations.[2,21−23] Although these techniques serve as key tools to observe and infer information about the dislocation structure, distribution and arrangement, they cannot provide accurate information on dislocation energetics and mobilities, which often govern the dislocations slip, slip-planes, and other dislocation-mediated phenomena such as macro scale ductility and crystal growth. From a modeling perspective, semicontinuum Peierls−Nabarro models[24,25] are extensively used to study dislocations by introducing the energies of generalized stacking faults from density functional theory to continuum model of the dislocations, yet the significant constraint of planar dislocations limits their applicability.[26] Alternative methods involve explicit calculation of the dislocation core structure using atomic scale simulations. In this category, fully periodic dipole approaches can be used to simulate an infinite array of dislocations (e.g., line defects in silicon,[8,9] extended defects in diamond cubic crystals,[27] and impurities at edge dislocations[7]); however, the correction for interactions between dislocation core fields[28,29] and contributions from core traction in the dislocation formation energy[30] make this method less straightforward for complex crystals. Recent development of the cluster embedded models[31,32] based on one-dimensional periodic boundary conditions opens the opportunity to systematically investigate

Received: August 20, 2014
Accepted: January 7, 2015
Published: January 7, 2015

DOI: 10.1021/am5091808
ACS Appl. Mater. Interfaces 2015, 7, 2223−2234

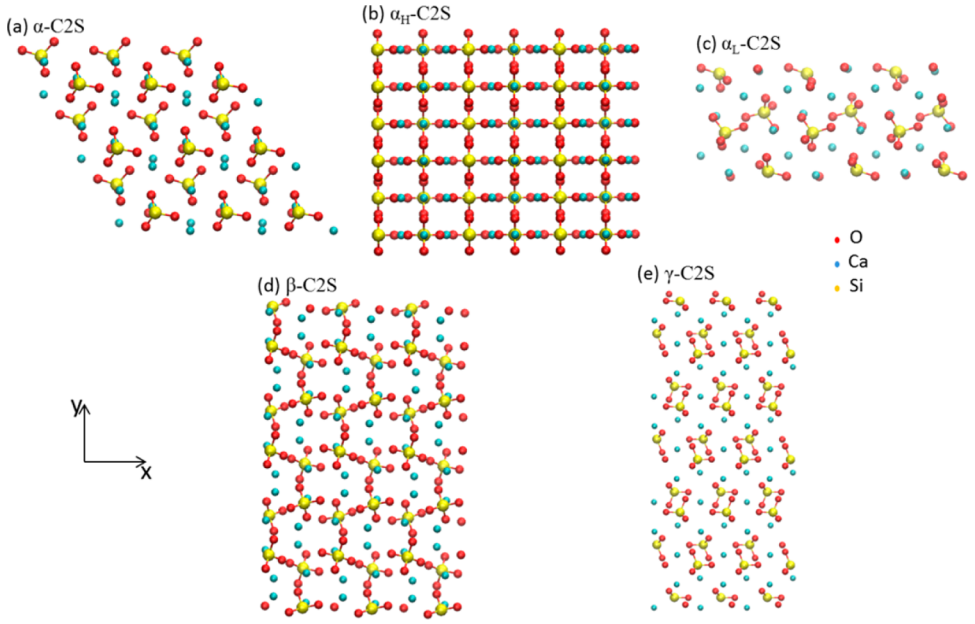

Figure 1. Atomic snapshots of dicalcium silicate polymorphs: (a) α-C_2S, (b) α_H-C_2S, (c) α_L-C_2S, (d) β-C_2S, and (e) γ-C_2S.

an isolated dislocation with atomic-scale fidelity. The cluster model, employed in this work, has already shown its success in predicting the core energy and structure of screw dislocations in different material classes including ionic materials (MgO),[32] zeolites,[33] wadsleyite minerals (β-Mg_2SiO_4)[34] and paracetamol (OH−-$C_6H_4NHCOCH_3$), a widely used drug more commonly known as acetaminophen.[32]

The objective of the present work is to study screw dislocations in structurally complex and low symmetry oxides, which are of both technological and scientific significance. We focus on five reversible polymorphs of dicalcium silicates (Ca_2SiO_3) as model systems. Ca_2SiO_3 is a key ingredient in industrial cement clinkers, and the defect characteristics and integrity of Ca_2SiO_3 crystal structures are absolutely critical in clinker grinding processes and crystal growth mechanisms.[35] The latter is of particular importance in hydration of dicalcium silicates to precipitate semicrystalline, nonstoichiometric calcium−silicate−hydrate (C−S−H) phase, which is the principal source of strength and durability of all Portland cement concretes.[35,36] Compared to tricalcium silicate (Ca_3SiO_5), the more dominant and energy-intensive component of the cement clinker, Ca_2SiO_3 (also known as belite with shortened notation of C_2S in cement chemistry) requires at least 100 °C lower temperature to produce but with the expense of more energy consumption for grinding it and slower reactivity with water, thereby leading to delayed strength development in cement paste.[37] However, given the overall economical gain due to the lower manufacturing temperature of Ca_2SiO_3 and the increased demand to reduce greenhouse emissions during cement manufacturing (currently cement manufacturing accounts for overall 5−10% of the worldwide CO_2 emissions), there is a growing interest to modulate grinding characteristics and reactivity of Ca_2SiO_3 to make it a more sustainable cement clinker. In this context, the knowledge of defects and screw dislocations can provide substantial information on how to tune and promote the salient properties of Ca_2SiO_3.

The crystal structure of dicalcium silicate is composed of SiO_4^{4-} tetrahedra and Ca^{2+} ions with a sequence of five reversible polymorphs, namely α, α_H, α_L, β, and γ, from high to low temperatures (Figure 1 and Figure S1, Supporting Information). We obtained the crystal and atomic structure of these polymorphs from X-ray experimental analysis.[38] These polymorphs can be transformed from one to another via changing the crystal symmetry, disorder of SiO_4^{4-} groups, and slight changes in the position of the Ca^{2+} atoms.[39−42] The α and β polymorphs have monoclinic crystal structures, while α_H, α_L, and γ polymorphs have orthorhombic crystal forms.[35]

Generally, dislocations in Ca_2SiO_3 arise from the growth and cooling processes during cement manufacturing, possibly affected by the presence of impurities.[43] Owing to variations in the size of the Burgers vector b, different crystal faces will behave differently during dissolution, etch pit formation, and hydration, which all depend on the type and density of dislocations.[43] Given the complexity of low-symmetry cement crystals, only very limited experiments are reported on the observation of dislocations,[44−47] and initiation of etch-pit formation from dislocations.[35,48] In this work, we focus at filling this gap by providing the first atomic-based understanding of the dislocation-mediated properties of Ca_2SiO_3 polymorphs, thereby offering de novo strategies for science-informed engineering of cement clinkers. Broadly, this approach will have important implications for mechanics and crystal growth processes of several other structurally complex materials such as microporous silicates and porous materials in general.

2. METHODS

Cluster Embedded Atom Model. We adopted a simulation strategy developed by Walker et al.[31] to combine an atomic scale model of the dislocation core with a description of the extended crystal based on continuum linear elasticity. The idea is to take advantage of the symmetry of Volterra dislocation to build a model using periodic boundary conditions along the dislocation line while only including a finite cluster of atoms perpendicular to the dislocation line. A convention in this study is to lay the screw dislocation line along the z axis.

A three-stage approach is taken to create the models of the screw dislocation. First, a charge neutral disk-shaped supercell containing the defect-free crystal structure is constructed in which the one-

DOI: 10.1021/am5091808
ACS Appl. Mater. Interfaces 2015, 7, 2223−2234

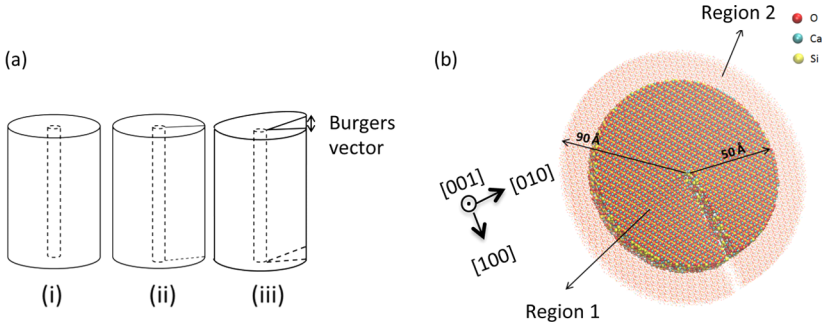

Figure 2. (a) Conceptual model of introducing screw dislocation based on linear elasticity. (b) Typical atomic illustration of the screw dislocation in dicalcium silicate. The atoms faded in color represent region 2, which is fixed during the energy minimization; (red) O, (blue) Ca, and (yellow) Si atoms.

dimensional periodicity passes through the central axis of the disk (z axis). The radius of the simulation cell is 90 Å to accommodate relaxation around the core, and its height is equal to the length of the Burgers vector, that is, one lattice constant along the z axis. The typical number of atoms in each simulation cell of the dicalcium silicate is around ~15 000−17 000.

Charge neutrality of the simulation cells is imposed by breaking the small extra charge (which is the result of cutting a cylinder from the supercell) to all the atoms (~15 000), thus leading to less than 1% change in the partial charge of each individual atoms. We assume this minimal change would not affect the accuracy of the force field predictions.

The second stage involves introducing the dislocation based on anisotropic linear elasticity.[49] Figure 2a shows the conceptual model of introducing a screw dislocation in a homogeneous linear elastic body, which involved three basic steps: (1) A small part in the center is removed because elastic theory has a singularity at the original point. This issue is not a major concern in the real atomic simulation cells due to the vacancies between the atoms, which could serve as the origin. (2) A solid line from the edge to the center of the cylinder is drawn to represent the "cut". The direction of this cut determines the x axis used in the mathematical formula of anisotropic elasticity. (3) Atoms at opposite sides of the cut are vertically displaced by a Burgers vector to form a screw dislocation. Note that for the cut surface to be indistinguishable, the crystal structure must be continuous across it, thus requiring that the Burgers vector must equal to one lattice vector.

In practice, the dislocated structure of the simulation cell in Figure 2a is constructed by the elastic displacement field, which maps the location of atoms in the bulk cell to the equivalent point in the dislocated cell. The elastic displacement field is only a function of Burgers vector, elastic properties of the crystals, and the atomic positions. For the monoclinic and orthorhombic crystals considered in this work, the displacement field is entirely parallel to the Burgers vector, that is, $\overline{b} = (0,0,b_z)$, and is given by[49]

$$u_x = u_y = 0$$

$$u_z = -\frac{b_z}{2\pi}\tan^{-1}\frac{(C_{44}C_{55} - C_{45}^2)^{1/2}y}{C_{44}x - C_{45}y} \quad (1a,b)$$

for monoclinic crystals, and by

$$u_x = u_y = 0$$

$$u_z = -\frac{b_z}{2\pi}\tan^{-1}\left\{\left(\frac{C_{55}}{C_{44}}\right)^{1/2}\frac{y}{x}\right\} \quad (2a,b)$$

for orthorhombic crystals. In eqs 1a,b and 2a,b, u_x, u_y, and u_z are atomic displacements due to the elastic theory; x, y, and z are the Cartesian atomic positions in the bulk cell; and C_{ij} are the components of the elastic tensor. Note that for monoclinic crystals, eq 1a,b is only valid when the axis perpendicular to parallelogram plane is parallel to the Burgers vector (z axis). Thus, all the results of this work related to the monoclinic α-C_2S and β-C_2S polymorphs pertain to this situation.

The final step needed to generate a model of the dislocation core is to allow the atoms to move to find a low energy configuration. Although the linear elastic displacement field is accurate for the atoms far away from the core, the energy minimization corrects for the nonlinear elasticity close to the core, allows the possibility of inhomogeneous strains, accounts for the atomic scale structure of the core, and allows the reconstruction if the core causes deformation of the surrounding crystal.[31] All energy minimizations in this work was performed using conjugate gradient algorithm as implemented in the GULP code.[50] To simulate the presence of the extended crystal, a 40 Å outer rim of the atoms was held fixed in the configuration predicted by the linear elasticity (region 2 in Figure 2b). Atoms within the 50 Å of the center of the cell were allowed to relax (region 1). The fact that the thickness of the region 2 is larger than the real space of the Coulomb cutoff radius ensures that the mobile atoms do not interact with the edge of the atomistic model.

To describe the interatomic interactions of dicalcium silicate polymorphs, we employed ClayFF force field potential.[51] This force field is based on an ionic−covalent description of metal−oxygen interactions and has been highly successful in predicting several structural and mechanical properties of crystalline minerals.[52,53] In ClayFF, metal−oxygen interactions are based on a simple 12−6 Lennard−Jones potential combined with Coulombic interactions. The empirical parameters and partial atomic charges are obtained from cluster and periodic density functional theory, quantum chemical calculations of simple oxide, hydroxide, and oxyhydroxide model compounds with well-defined structures. Using this force field, the extraction of the elastic constants and Young moduli from atomistic simulations is straightforward by calling the property calculation option in GULP. For instance, elastic constants are obtained by taking the second derivative of energy density with respect to strains. The detailed parameters of ClayFF potential in given in Tables S1 and S2 (Supporting Information), and the comparison of its predictions with experiments for lattice parameters and elastic properties of C_2S polymorphs are given in Tables S3−S5 (Supporting Information).

Calculation of Dislocation Formation Energy and Dislocation Core Radius. Once an energy minimum has been obtained, various techniques described below are used to explore the structural and energetic characteristics of the core. In this context, one important piece of information is a measure of the thermodynamic stability of the dislocation, or the dislocation formation energy, which is defined as the work (per unit length) required to introduce a dislocation to a bulk. The existence of a distortion due to dislocation makes the total dislocation formation energy a combination of two parts: the energy of the dislocation core and the elastic energy of the extended crystal system as a result of the dislocation core. Note that in contrast to the point or planar defects, there is no unique dislocation formation energy per unit length of dislocation. The formation energy includes an elastic part arising from elastic strain distributed across the extended crystal and thus is a function of the size of the crystal from the

DOI: 10.1021/am5091808
ACS Appl. Mater. Interfaces 2015, 7, 2223−2234

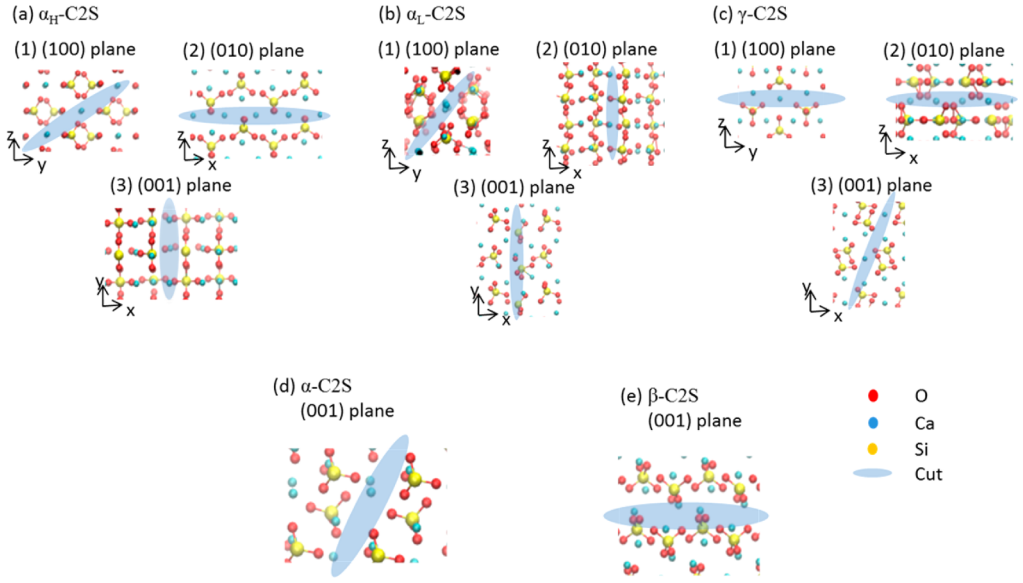

Figure 3. Schematic representation of "cut" orientation in dicalcium silicate polymorphs; (a–c) three orthorhombic crystals where three screw dislocations are studied; (d and e) monoclinic crystals in which only the dislocation perpendicular to parallelogram plane is investigated.

dislocation line. The total formation energy, E, stored within a cylindrical crystal of radius r is given by[49]

$$E(r) = E_{\text{core}} + \frac{Xb^2}{4\pi} \ln\left(\frac{r}{r_0}\right) \tag{3}$$

where r_0 is the size of the dislocation core with energy E_{core}, b is the length of the Burgers vector as before, and X is an energy factor depending on the symmetry of the elastic constant tensor and equal to shear modulus in isotropic materials.

There are two unknowns in eq 3, E_{core} and r_0, which can be determined by calculating $E(r)$ for various radii. To do so, the cell derived from the energy minimization is divided into two regions. Region 1 contains the atoms found inside a certain radius, r, and region 2 is the rest of atoms outside of the region 1 (conceptually similar to regions shown in Figure 2b). Then, the energy of the simulation cell containing the dislocation is partitioned into three parts: (1) interactions between atoms within region 1, E_d^{11}, (2) interactions between atoms in region 2, E_d^{22}, and (3) interactions between the two regions, E_d^{12} or E_d^{21}. Equivalently, the energies in the perfect crystal can be partitioned in the same way as E_p^{11}, E_p^{12} (or E_p^{21}) and E_p^{22}. Then, the dislocation formation energy stored within region 1 is given by[20]

$$E(r) = [E_d^{11} + E_d^{12}] - [E_p^{11} + E_p^{12}] \tag{4}$$

where $E(r)$ is calculated for various radii and the resulting data is fitted to eq 3 to obtain E_{core} and r_0. Note that due to geometry optimization, which may lead to radial displacements, the atoms in region 1 in bulk cell may not be within the same cutoff radius in the dislocated structure. Tracking atomic movement is critical to ensure that E_d^{11} contains an identical number of atoms in both the bulk and dislocated cells. It is worth noting that for materials with low symmetry, the parameter X can also be left as an unknown for an overall better fit, making the total number of unknowns three. Then, after fitting, the close agreement of the X parameter with the average shear modulus of the crystals obtained from the Reuss–Voigt–Hill method[54] ensures the accuracy of the method.[32]

Calculation of Peierls Stresses. Another important quantity related to the dislocation is the Peierls stress, which is the force needed to move a dislocation at 0 K within a plane of atoms in the unit cell. Generally speaking, Peierls stress can be obtained through pure shear simulation and it is defined as the stress at which point the dislocation starts to move.[55] Here, we applied shear stress to the system via MD simulations implemented in LAMMPS code at 1 K (LAMMPS code does not accept 0 K) to obtain the required stress (Peierls stress) that moves the dislocation. More precisely, for each polymorph, the system is first relaxed in the microcanonical ensemble (NVE) for 10 ps at 1 K to ensure the convergence of the energy and volume. Then, various shear stresses are applied in either side of the slip plane, for example, (010) plane in Figure 2b, and further MD simulations are carried out in NVE ensemble for 100 ps. Next, by identifying the onset of yielding in the shear stress versus shear strain diagram, we identified the required stress, that is, the Peierls stress, that results in dislocation movement. For all MD simulations, we used a time step of 1 fs.

RESULTS AND DISCUSSION

Figure 3 shows the orientation of the chosen cut within the in-plane direction of each Ca_2SiO_3 polymorph. The orientation of these cuts usually lies along a channel to avoid any Si–O bond breakage, and the orientation strongly depends on the plane symmetry. Note that the displacement of two sides of the cut is exactly one Burgers vector (perfect dislocation). The final atomic structures of the dislocated crystals were found by applying the linear elastic theory to the simulation cell with the preferred cut, followed by energy minimization. As an example, Figure 4 shows the original structure, approximated elastic configuration, and the final atomically optimized structure of [100] screw dislocation in α_H-C_2S. Generally, the core appears in a spiral shape, as shown in Figure 4b,c. Note that due to periodicity along the dislocation line, the dislocated structure is not clearly visible in Figure 4c. However, the green shaded band on the right side of Figure 4 denotes the atoms that were located in the same plane in the perfect crystal before the dislocation was introduced.

Geometry of the Dislocation Core. Once the dislocated structure has been established and minimum energy configuration is achieved, it is possible to describe the dislocation core characteristics in several ways. On the shortest scale, the bonding and atomic structure close to the core are analyzed. Interestingly, some crystals undergo a dramatic rearrangement around the core while some retain a similar planar configuration. As an example, Figure 5 demonstrates the core structure of the dislocated α-C_2S and three dislocated core structures of α_H-C_2S in the (100), (010), and (001) planes.

DOI: 10.1021/am5091808
ACS Appl. Mater. Interfaces 2015, 7, 2223–2234

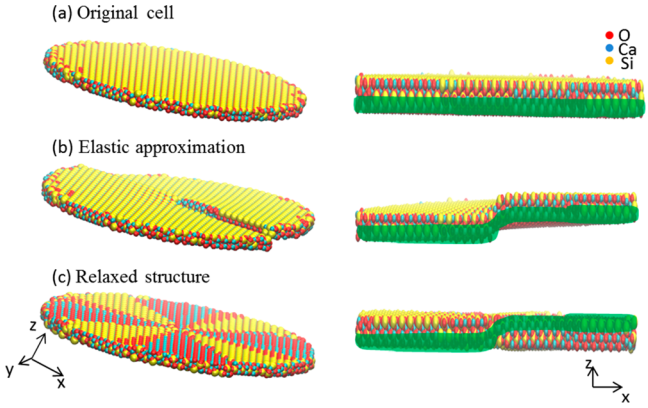

Figure 4. (a) Original structure, (b) dislocated structure via elastic theory, and (c) atomically relaxed structure of [100] screw dislocation in αH−C_2S.

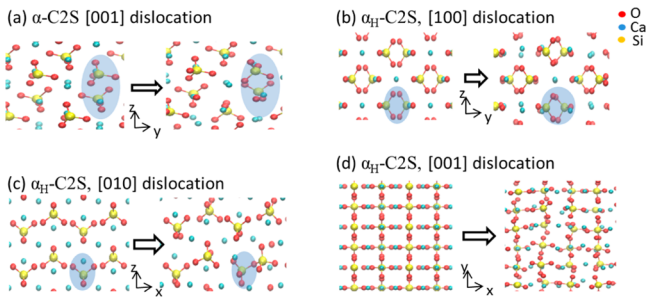

Figure 5. Comparison of atomic positions and orientations in the (left) original and (right) dislocated structures of α-C_2S and three orthogonal planes of α_H-C_2S. These pictures are close-up views from an identical angle at the final core structures along the dislocation line. Note that in panels a−c, the z axis is in the plane of the image, whereas in panel d the image is viewed from the z axis.

This figure provides a comparative view of the atomic positions in the original and dislocated structures. In the case of [001] dislocation of α-C_2S (Figure 5a), while the structure of tetrahedra remains complete and independent in both the original and dislocated cells, the relevant positions and orientations are changed significantly (albeit, in a rigid-body type deformation to be discussed later) due to distortion imposed by the dislocation core. In light of eqs 1a,b and 2a,b, the linear elastic estimation indicates zero displacement radially. Therefore, all the in-plane movements shown in Figure 5 are due to atomic relaxation enforced by nonlinear elasticity around the core. Two tetrahedra shaded in blue in Figure 5a clearly show their relevant in-plane movements as well as self-rotations. However, the average Si−O bond lengths and the average O−Si−O bond angles almost do not change, which will be quantitatively discussed later.

The rearrangement resulting from the [100] dislocation core in α_H-C_2S (Figure 5b) is not as significant as that in α-C_2S. There is negligible self-rotations, and the groups of tetrahedra facing each other get only slightly closer. In the case of [010] core dislocation in α_H-C_2S (Figure 5c), there are considerable rotations in the silicon tetrahedra and the magnitude of these rotations depends on the angles between the chain-like silicon tetrahedra and the dislocation line. Additionally, the shaded tetrahedra exhibit small in-plane movements. However, overall, the alignment of the tetrahedral backbone is preserved. The original (001) plane in Figure 5d has a more closely packed structure than the (100) and (010) planes, leading to significant atomic displacements and rotations upon dislocation.

Differential Displacements and Core Expansions. On a slightly larger length scale, an efficient way of examining the structure of the dislocation core is by plotting the differential displacements of adjacent atoms along the dislocation line. Arrows are plotted between the neighboring atoms with length proportional to Δu_z. This representation clearly demonstrates when a screw dislocation spreads onto one or more planes and allows visualization of such processes. Furthermore, the expanding directions of the arrows indicate the low Peierls stress directions where the core is more likely to glide along those directions.[56] This idea comes from studies on body centered cubic (bcc) metals where the core is suggested to appear in two forms, a nonplanar core that is immobile under stress and a planar core that can move on a particular slip plane. By using the cluster model, a nonplanar core could be captured, which is not possible via classical Peierls−Nabarro (PN) model[20,24] where the core is a priori chosen to be planar. Although there are techniques that side-step this limitation of the PN model,[57,58] the cluster model is a relatively simple and efficient method in this context.

Figure 6 shows the differential displacements of [100], [010], and [001] dislocations in α_H-C_2S as an example (the differential displacements of other polymorphs are given in Figures S2−S4, Supporting Information). Arrows are plotted between adjacent Si atoms (yellow dots) in identical original planes. The length of arrows are scaled to the value of each Burgers vector. Figure 6a−c clearly shows that the dislocation core spreads onto one or more planes, and the expanding shape is very different in three mutually perpendicular planes. For [100] dislocation, the core exhibits a rather isotropic, elliptic spread that stretches ∼28 Å along the [001] direction and ∼22 Å along the [010] direction. However, the areas of core spreading under the [010] and [001] dislocations are concentrated on a few layers, especially the core of the [001] dislocation localized in a narrow band extending to ∼45 Å along the [100] direction. Note that to obtain the core expansion, one can also evaluate the disregistry function and fit the data to arctan function in classical PN model (Figure S5, Supporting Information); however, as discussed above, the core expansion will be planar, as opposed to differential displacement method, which give information on nonplanar core expansions.

Core Displacement Fields. On the largest length scale, it is appropriate to consider the movement of atoms during the geometry optimization. These movements can be split into parallel and perpendicular to the dislocation line, and arise from the fact that the linear elasticity is not sufficient to describe the dislocation core structure. Figure 7 shows the core displacement fields of [100], [010], and [001] dislocations in α_H-C_2S. In view of this figure, several important observations are in order.

First, because Figure 7 illustrates the vertical and radial displacements of atoms before and after energy relaxation, it represents a good check-point to test the validity of the thickness of region 1 (chosen 50 Å), which serves as an active region to bear the influence of the dislocation. In other words, the fix boundary conditions in region 2 are valid only when all the perturbances occur in region 1. From Figure 7, it appears that both the vertical and radial displacements rapidly decay when approaching region 2 at r ∼ 50 Å.

Second, Figure 7 reveals that the model crystal is not a linear elastic continuum in all the three directions. In particular, there

DOI: 10.1021/am5091808
ACS Appl. Mater. Interfaces 2015, 7, 2223−2234

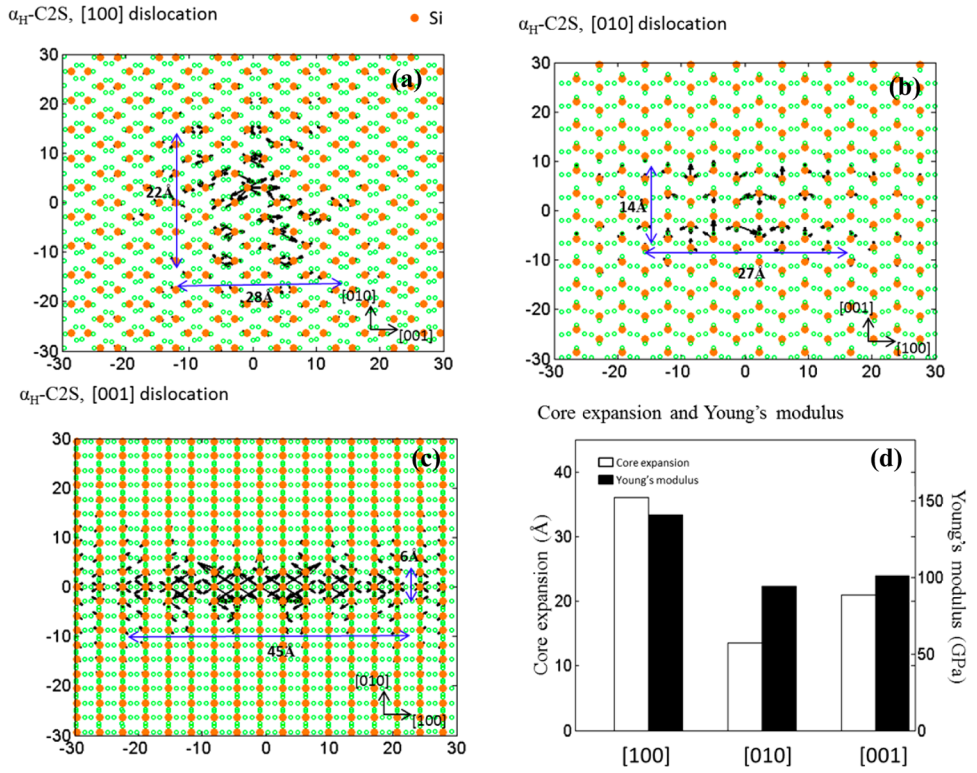

Figure 6. Differential displacements of α_H-C_2S under (a) [100] dislocation, (b) [010] dislocation, and (c) [001] dislocation. Arrows indicate the displacement in the z direction (not in-plane). (d) Young's moduli and average core expansions along three orthogonal directions of α_H-C_2S.

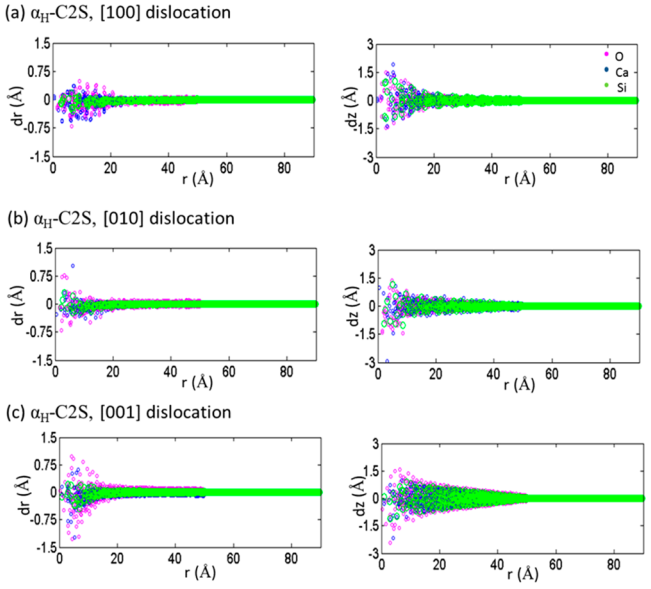

Figure 7. (left) Radial and (right) vertical core displacement fields of three screw dislocations in α_H-C_2S due to energy minimization; (a) [100], (b) [010], and (c) [001].

is a significant radial displacements within the 20 Å of the core, whereas the linear elasticity (eqs 2a,b and 3) suggests zero in-plane movements. In all three directions, the movements are dominated by O and Ca atoms (vs Si atoms).

Third, the [001] dislocation leads to the most displaced structure (Figure 7c). This might be intuitively expected because of its largest Burgers vector among the three directions; b = 7.205, 5.872, 9.245 Å for [100], [010], and [001] directions, respectively. Atoms far away from the core experience relatively large displacements during energy minimization. This significant repositioning happens in the most closely packed plane, the (001) plane, and can be explained by realizing the differences in the planar core structures shown in Figure 5b–d. The channel space in the (010) plane (Figure 5b) and (100) plane (Figure 5c) "take away" the torsion from dislocation and reduce the interactions among tetrahedra. Therefore, the energy minimum can be achieved easily. However, the ordered pattern of atoms in Figure 5d indicates significant interactions among neighboring tetrahedra, and these interactions propagate so fast that even atoms far away from the core are influenced.

Fourth, from Figure 7c it appears that the majority of the radial displacements are inward, toward the dislocation core (more points have negative dr). This can be explained as follows. Consider a circle lying around the dislocation line in α_H-C_2S. Upon introduction of screw dislocation via elastic theory, this circle becomes a helix with the same radius (the elastic theory only vertically displaces atoms). This helical shape entails larger separations between atoms located around the circumference of the helix compared to the separations in the original crystal structure (the circumference of a helix is simply larger than that of a circle with the same radius). One way to reduce this imposed distortion and bring the atoms closer to the equilibrium positions is to reduce the radius of the helix compared to that of a circle. This reduction can be achieved by inward motion of the atoms around the dislocation line during energy minimization. In fact, the smaller dislocated volume results in less strain to the rest of the system as well. Similar pattern of inward motions have been observed for screw dislocations in MgO, forsterite,[32] zeolite A[33] and wadsleyite.[34] Generally, other polymorphs of dicalcium silicate exhibit similar

DOI: 10.1021/am5091808
ACS Appl. Mater. Interfaces 2015, 7, 2223–2234

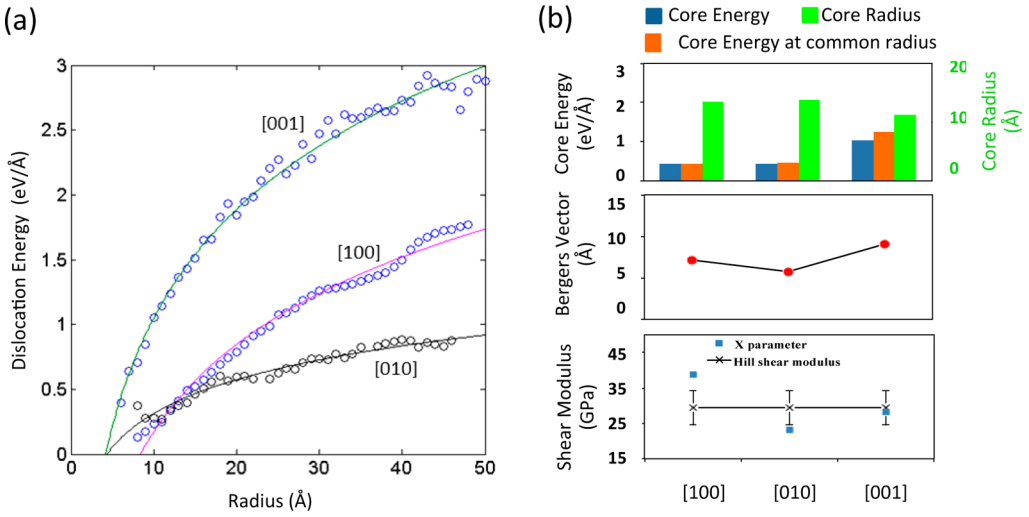

Figure 8. (a) Dislocation formation energy as a function of radius from dislocation line for [100], [010], and [001] dislocations in α_H-C_2S. The solid lines denote the fitting result of eq 3 to the scattered points. (b) Comparisons of core energy, core radius, core energy at a common radius of 14.2 Å, Burgers vector, fitting parameter X and the average shear modulus for [100], [010], and [001] dislocations in α_H-C_2S. The bars on the shear moduli indicate the lower and upper bounds from the Reuss−Voigt−Hill method.

trends and observations associated with core displacement fields (Figures S6−S8, Supporting Information).

Dislocation Core Energy. Figure 8a demonstrates the dislocation formation energy of α_H-C_2S as a function of radius. This energy is, in general, a logarithmic function of distance (r) from the dislocation line. Clearly [001] direction has a larger dislocation formation energy than the [100] and [010] directions. Figure 8b shows the magnitudes of the core energies and core radii, which are extracted by fitting eq 3 to the scattered data. For reference, the Burgers vector and the fitted X parameters are also shown in the plot. For comparison of dislocation core energies at different crystallographic directions, core energies must be evaluated to a common radius (as opposed to direct extraction of core energies obtained from the fit of eq 3, which correspond to different core radii).[59] Thus, in Figure 8b we have also shown the dislocation core energies for a common radius of 14.2 Å, which is the largest radius among the three core radii (Table 1). As expected, the core energies increase for the cases that their radii are smaller than the common radius.

Table 1. Core Energies and Core Radii of α-C_2S

	[100]	[010]	[001]
core energy (eV)	0.45	0.432	1.033
core energy at a common radius of 14.2 Å (eV)	0.45	0.4517	1.25
core radius (Å)	14.2	13.71	11.19

Given a common radius of 14.2 Å, the smallest core energy is 0.45 eV/Å under the [100] dislocation. This indicates that a new screw dislocation is more likely to occur in a [100] direction. In other words, a [001] screw dislocation is unlikely due to its large core energy, which entails more bond breakages and reconstructions in compared to other two directions. However, this correlation may not necessarily be true among different polymorphs. The core energies and core radii of all dicalcium silicate polymorphs are calculated and given in Figure 9. For a common radius of 14.53 Å, while α-C_2S has 23 and 37% larger Burgers vector compared to α_L-C_2S and γ-C_2S,

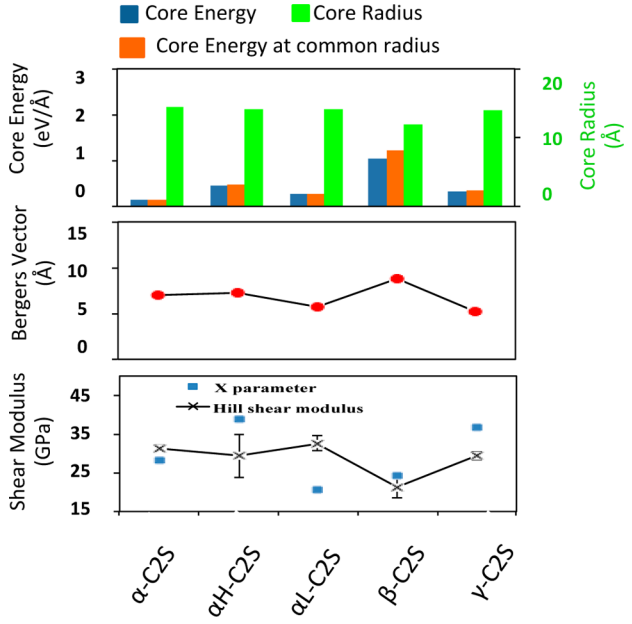

Figure 9. Comparisons of core energy, core radius, core energy at a common radius of 14.53 Å, Burgers vector, fitting parameter X, and the average shear modulus for all dicalcium silicate polymorphs. The bars on the shear moduli represent the lower and upper bounds based on Reuss−Voigt−Hill method. For each orthorhombic crystal (α_H-C_2S, α_L-C_2S,γ-C_2S), only the directions associated with the smallest formation energy are shown, that is, [100] for α_H-C_2S, [001] for α_L-C_2S, and [100] for γ-C_2S.

respectively, its core energy is 47 and 57.2% less compared to α_H-C_2S and α_L-C_2S (Table 2), owing to the large channel and free rigid-body type movements of Si tetrahedra (to be discussed shortly), which take away the majority of the distortion imposed by screw dislocation. Therefore, in spite of the common intuition based on simple crystalline materials that the larger the Burgers vector, the higher the core energies, we found that this is not necessarily the case for low symmetry dicalcium silicate polymorphs due to the complicated atomic arrangement around the dislocation core. Nevertheless, the

DOI: 10.1021/am5091808
ACS Appl. Mater. Interfaces 2015, 7, 2223−2234

Table 2. Core Energies and Core Radii of Different C_2S Polymorphs

	α-C_2S	α_H-C_2S	α_L-C_2S	β-C_2S	γ-C_2S
core energy (eV)	0.15	0.45	0.275	1.033	0.33
core energy at a common radius of 14.53 Å (eV)	0.15	0.473	0.2835	1.218	0.351
core radius (Å)	14.53	14.2	14.17	11.9	14.00

crystals with larger core energies have generally smaller dislocation core radii.

Among all dicalcium silicate polymorphs, α-C_2S and β-C_2S have the smallest and largest core energies (at a common radius), respectively, which in part may be due to their internal crystal atomic structures. More precisely, although Si tetrahedral and Ca ions move due to dislocation distortion, the analysis of bond lengths and bond angles on the nearest neighbor shell of the dislocation core shows that in α-C_2S, the average bond lengths and angles are almost identical before and after dislocation, suggesting nearly rigid-body type movements in between the large channel (Figure 10). This justifies the lowest value of the dislocation core energy in α-C_2S (i.e., no actual bond stretches). However, in β-C_2S, Ca ions move rather significantly before and after dislocation to minimize the imposed strain of the dislocation, but still, Ca−Si and Ca−O bond lengths are stretched considerably, resulting in higher dislocation energy in β-C_2S. Similar trends and discussions are valid for other dicalcium silicate polymorphs (Figures S9, Supporting Information). For comparison, the energies of the C_2S polymorphs without dislocations are also given in Table S6 (Supporting Information).

It is interesting to note that the fitted value of X parameters (Figures 8b and 9) match very well with the average shear modulus calculated from the Reuss−Voigt−Hill approach (Supporting Information), which is the most common method for averaging elastic properties of anisotropic crystals.[54] This means that eq 3, a closed form formula derived from complete radial symmetry, is still applicable to low symmetry crystals in spite of various anisotropies associated with their elasticity. We speculate that this wide applicability is due to the existence of complex, competing mechanisms in low symmetry crystals that may cancel each other out or are averaged out through the dislocation process and energy minimization.

Relation Between Dislocation Core Expansions and Young's Modulus. To better understand the dislocation core features, we show the Young's moduli and the average core size expansions of α_H-C_2S in three orthogonal directions in Figure 6d. For example, the 36 Å core expansion along [100] axis is an average of 27 and 45 Å core expansions along the [010] and [001] directions, respectively. Similar plots for α_L-C_2S and γ-C_2S are given in Figures S2d and S3d (Supporting Information). The comparison of core spreading and Young's moduli in Figure 6d and Figures S2d and S3d (Supporting Information), reveals an interesting observation, that is, the core of the screw dislocations tends to expand more toward the directions with higher Young's moduli. The underlying reason goes back to the packing of atomic species, which dictates the strength of atomic bonds and consequently Young's moduli. In other words, the directions with higher Young moduli are more sensitive to defects since the impact of core disturbance can be transported to further distances through strong connectivity of atomic species.[10]

Impacts on Grinding Energy and Crystal Growth. The knowledge of dislocation mobilities can provide essential information on the inherent materials features such as brittleness and ductility, which can influence the fracture and grinding mechanisms of cement clinkers. Figure 11a−c shows the shear stress−strain relationships obtained via MD simulations at 1 K for the three orthorhombic polymorphs. In each case, for a small external stress, the shear stress−strain relationship is almost linear. However, as the external stress increases, it causes the dislocation to move (the onset of yielding). This is reflected by the intersection of the two linear lines fitted to the linear and nonlinear parts of the stress−strain curves, corresponding to the Peierls stresses, which are associated with different [100], [010], and [001] dislocations lines (e.g., for [001] dislocation line, the Peierls stress lies in the (010) plane, as shown in Figure 2b). By definition, larger Peierls stress reveals a more brittle material, that is, lower mobility.[60] By comparing Figure 11, it turns out that while the brittleness of α_H-C_2S and α_L-C_2S is rather insensitive to the crystallographic directions, there is a strong dependence of Peierls stress (and thus brittleness) of γ-C_2S on crystallographic directions. More precisely, it is easier to fracture and grind γ-C_2S when the dislocation line is along [001].

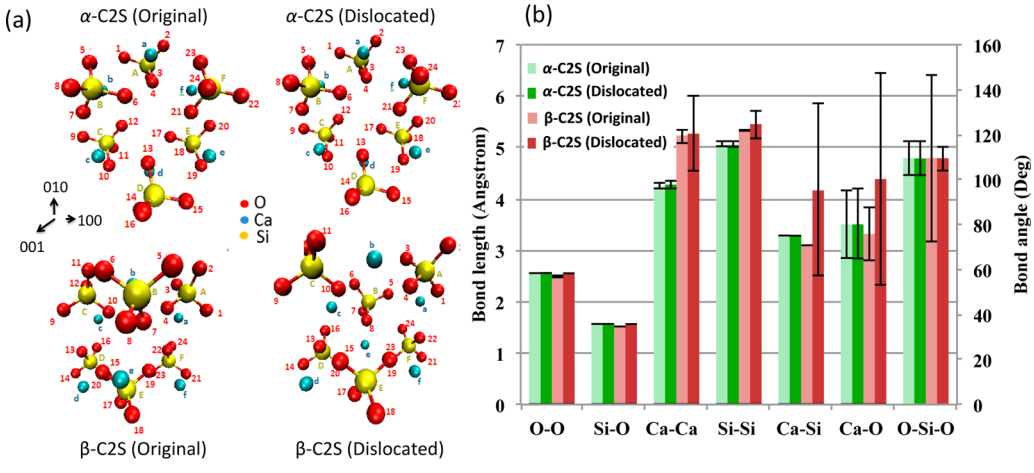

Figure 10. (a) Atomic structure of the nearest neighbor shell around the dislocation line in α-C_2S and β-C_2S. (b) Average bond lengths and angles in the original and dislocated structure; bars indicate standard deviations.

DOI: 10.1021/am5091808
ACS Appl. Mater. Interfaces 2015, 7, 2223−2234

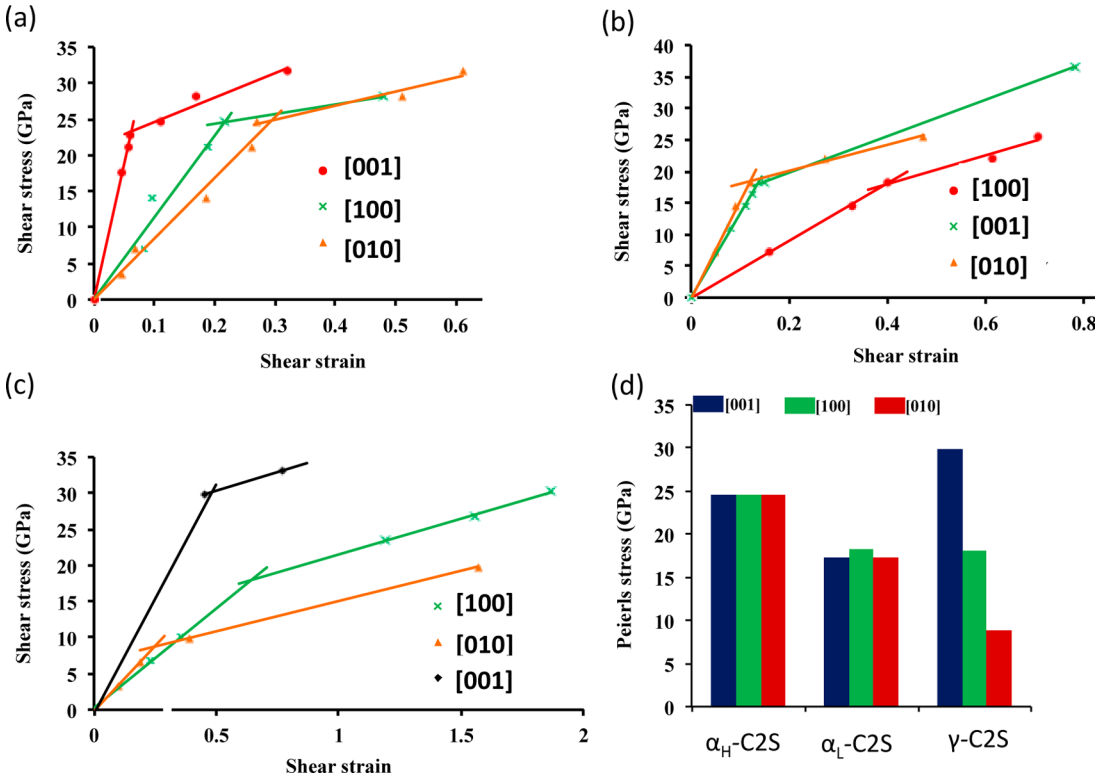

Figure 11. Shear stress–strain relationships for orthorhombic (a) α_H-C_2S, (b) α_L-C_2S, and (c) γ-C_2S along the [100], [010], and [001] screw dislocations. The intersection of the two fitted linear curves correspond to the Peierls stress (yielding point), which causes the dislocations to move. (d) Peierls stress values for the polymorphs in panels a–c associated with [100], [010], and [001] dislocation lines.

Figure 12 and Table 3 show shear stress–strain relations and the Peierls stresses for all polymorphs of dicalcium silicate.

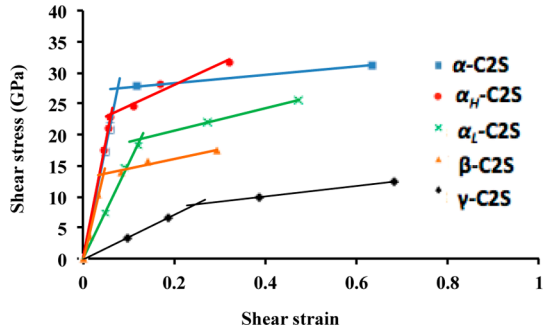

Figure 12. Shear stress–strain relationships for all dicalcium silicate polymorphs. For orthorhombic polymorphs (α_H-C_2S, α_L-C_2S, and γ-C_2S), only the directions with lowest Peierls stress are shown. The intersection of the two fitted linear curves correspond to the Peierls stress (yielding point), which causes the dislocations to move.

Table 3. Peierls Stress for Screw Dislocations in Dicalcium Silicate Polymorphs[a]

dicalcium silicate	Peierls stress (GPa)
α-C_2S	27.14
α_H-C_2S	24.60
α_L-C_2S	17.27
β-C_2S	13.90
γ-C_2S	8.92

[a]For orthorhombic polymorphs (α_H-C_2S, α_L-C_2S, and γ-C_2S), only the lowest Peierls stresses are shown.

Note that for orthorhombic polymorphs (α_H-C_2S, α_L-C_2S, and γ-C_2S), only the directions with lowest Peierls stress are shown because those directions will be hot spots in mechanical loading that yield prior to other directions. Among different polymorphs in Figure 12, α-C_2S has the highest Peierls stress indicating that the dislocations in α-C_2S rarely move. Thus, the crystal should manifest brittle characteristics. In this context, α_H-C_2S ranks second with slightly lower Peierls stress, and other polymorphs exhibit relatively smaller Peierls stresses. Indeed, Table 3 could provide important information and insights for optimizing grinding processes of Ca_2SiO_3 clinkers in cement plants. In light of the fact that a brittle crystal is favored during grinding processes (it breaks rapidly and requires less energy), we propose cement manufacturers to focus on more grinding α-C_2S (or α_H-C_2S) polymorphs rather than other polymorphs. Although α-C_2S and α_H-C_2S are thermodynamically stable at temperatures higher than room temperature, cement manufacturers can tune the clinker cooling processes to find a balance between the savings in the grinding energy and the (potential) thermal energy required for stability of these polymorphs to find an overall optimum solution. To our knowledge, this work is the first report on estimating brittleness and associated grinding energy of dicalcium silicate polymorphs based on atomic-level information. We reiterate that all our observations in this manuscript are based on screw dislocations alone. Thus, future studies on edge-dislocation mechanisms, twining deformations and their interactions with dislocations can potentially provide more refined data on brittleness and grinding solutions for C_2S polymorphs.

Finally, we turn our attention to the reactive properties of the core and how the screw dislocation may impact the

DOI: 10.1021/am5091808
ACS Appl. Mater. Interfaces 2015, 7, 2223–2234

mechanisms of crystal growth, such as the growth of calcium-silicate-hydrate (C−S−H) phase, the key hydration product of Ca_2SiO_3 that is responsible for mechanical properties of cement pastes. It is known that the discontinuity caused by screw dislocations in Ca_2SiO_3 serves as a basin for water molecules, and the hydration process might be expedited by increasing screw dislocation density.[43] Screw dislocations with smaller core energy form easier and multiply faster upon deformation,[49] thereby providing more hot spots for dissociation and crystal growth. In light of Figure 8b and Figure 9, it appears that the following directions are energetically preferred for crystal growth due to their relatively low dislocation core energies: [010] direction in α_H-C_2S, [001] direction in α_L-C_2S, and [100] direction in γ-C_2S (although the latter polymorph does not widely exist in real clinker due to required stabilization by guest ions). More importantly, our findings suggest that α-C_2S and β-C_2S have respectively the highest and lowest reactivity among all Ca_2SiO_3 polymorphs. These finding match extremely well with experimental evidence reporting identical rankings for reactivity of Ca_2SiO_3 polymorphs when mixing with water.[61] Besides the dislocation core energy, atomistic simulations have shown that the steps and topology of the core also influence the crystal growth and energetics of the major adsorbate sites, which are typically around the core geometry in screw dislocations terminated at a surface.[62] Thus, when searching for reaction accelerators (inhibitors), it will be useful to identify those adsorbates that bind and dissociate (block) the dislocation core sites.

CONCLUSION

We studied the atomic-scale characteristics of screw dislocation in five polymorphs of dicalcium silicate as a class of complex low symmetry oxides. Unlike the common intuition base on simple crystalline materials that the larger the Burgers vector, the higher the core energies, we found that this is not necessarily the case for low symmetry dicalcium silicate polymorphs. Instead, we found that α-C_2S has the lowest core formation energy and thus the most favorable dislocation in dicalcium silicates, mainly due to the large channels and nearly rigid body type movements of atoms, which take away majority of the distortion imposed by screw dislocation.

Equally important, by estimating the Peierls stresses by shear simulations of the system, we identified the following order in terms of relative brittleness (base on screw dislocation only), which is most favorable for grinding dicalcium silicates: α-C_2S > α_H-C_2S > α_L-C_2S > β-C_2S > γ-C_2S. The knowledge of the latter can significantly influence micro cracking, brittleness, and fracture, and can help devise strategies to reduce the energy associated with grinding dicalcium silicate (cement) clinkers.

Finally, we found that while α-C_2S is the most reactive polymorph in dislocation-mediated crystal growth, β-C_2S is the least reactive polymorph due to its highest screw core formation energy among dicalcium silicates. Generally, our analysis suggest the following order for reactivity: α-C_2S > α_L-C_2S > γ-C_2S > α_H-C_2S > β-C_2S. This information, combined with the predicted grinding efficiencies, can provide valuable insights and guiding hypotheses for experimentalists to tune the cement grinding mechanisms and reactivity processes for an overall optimum solution with regard to both energy consumption and performance. This is the most significant result of this paper and can provide crucial insight for intelligent synthesis, isolation, and tuning of ideal polymorphs in structurally complex systems with thermodynamically reversible polymorphs. To the best of our knowledge, this work is the first report of atomistic-scale analysis of dislocations in structurally complex dicalcium silicates, and can potentially open up several new opportunities for further studies, such as edge dislocation-mediated mechanisms, brittle-to-ductile transitions, and twinning deformations and their interactions with dislocations, to provide a comprehensive understanding of deformation mechanisms in cement clinkers. Broadly, the methods and strategies of this work can impact several other oxides and low-symmetry crystals such as jennite[36] and calcio-silicate layered materials,[63−65] as well as recently developed realistic and combinatorial models of calcium−silicate−hydrates[66−68] and microporous materials in general.[69,70]

ASSOCIATED CONTENT

Supporting Information

Force field parameters, force field predictions of lattice parameters and elastic properties, differential displacements and core displacements of various dicalcium silicate polymorphs, disregistry functions and their derivatives, and Reuss−Voigt−Hill approach to calculate the average shear modulus for anisotropic crystals. This material is available free of charge via the Internet at http://pubs.acs.org.

AUTHOR INFORMATION

Corresponding Author

*E-mail: rouzbeh@rice.edu.

Author Contributions

R.S. designed the research; R.S and L.C performed the simulation and theoretical work; R.S and L.C. analyzed the data; and R.S. wrote the paper.

Notes

The authors declare no competing financial interest.

ACKNOWLEDGMENTS

R.S. acknowledges the financial support by the National Science Foundation, award numbers 1235522 and 1346506. We are thankful to Mr. Lei Tao for help in calculation of Peierls stresses via MD simulations. The use of supercomputer machines for this work was supported in part by National Institutes of Health Award No. NCRR S10RR02950 and an IBM Shared University Research (SUR) Award in partnership with CISCO, Qlogic, and Adaptive Computing, and in part by the Data Analysis and Visualization Cyber infrastructure funded by NSF under Grant No. OCI-0959097.

REFERENCES

(1) Smereka, P. Spiral Crystal Growth. *Phys. D* **2000**, *138* (3−4), 282−301.

(2) Hull, D.; Bacon, D. J. *Introduction to Dislocations*. 4th ed.; Butterworth−Heinemann: Oxford, 2001.

(3) Sinclair, J. E. Improved Atomistic Model of a bcc Dislocation Core. *J. Appl. Phys.* **1971**, *42*, 5321−5329.

(4) Gehlen, P. C.; Hirth, J. P.; Hoagland, R. G.; Kanninen, M. F. A New Representation of the Strain Field Associated with the Cube−Edge Dislocation in a Model of a α-Iron. *J. Appl. Phys.* **1972**, *43*, 3921−3933.

(5) Ismail-Beigi, S.; Arias, T. A. Ab Initio Study of Screw Dislocations in Mo and Ta: A New Picture of Plasticity in bcc Transition Metals. *Phys. Rev. Lett.* **2000**, *84*, 1499−1502.

(6) Yang, L. H.; Söderlind, P.; Moriarty, J. A. Accurate Atomistic Simulation of (a/2) ⟨111⟩ Screw Dislocations and Other Defects in bcc Tantalum. *Philos. Mag. A* **2001**, *81*, 1355−1385.

DOI: 10.1021/am5091808
ACS Appl. Mater. Interfaces 2015, 7, 2223−2234

(7) Kaplan, T.; Liu, F.; Mostoller, M.; Chisholm, M. F.; Milman, V. First-Principles Study of Impurity Segregation in Edge Dislocations in Si. *Phys. Rev. B* **2000**, *61*, 1674−1676.
(8) Liu, F.; Mostoller, M.; Milman, V.; Chisholm, M. F.; Kaplan, T. Electronic and Elastic Properties of Edge Dislocations in Si. *Phys. Rev. B* **1995**, *51*, 17192−17195.
(9) Bigger, J. R. K.; McInnes, D. A.; Sutton, A. P.; Payne, M. C.; Stich, I.; King-Smith, R. D.; Bird, D. M.; Clarke, L. J. Atomic and Electronic Structures of the 90° Partial Dislocation in Silicon. *Phys. Rev. Lett.* **1992**, *69*, 2224−2227.
(10) Heggie, M. I.; Ewels, C. P.; Martsinovich, N.; Scarle, S.; Jones, R.; Goss, J. P.; Hourahine, B.; Briddon, P. R. Glide Dislocations in Diamond: First-Principles Calculations of Similarities with and Differences from Silicon and the Effects of Hydrogen. *J. Phys.: Condens. Matter* **2002**, *14*, 12689.
(11) Martsinovich, N.; Heggie, M. I.; Ewels, C. P. First-Principles Calculations on the Structure of Hydrogen Aggregates in Silicon and Diamond. *J. Phys.: Condens. Matter* **2003**, *15* (39), S2815.
(12) Rabier, J.; Soullard, J.; Puls, M. P. Atomistic Calculations of Point-Defect Interactions with an Edge Dislocation in NiO. *Philos. Mag. A* **1990**, *61*, 99−108.
(13) Rabier, J.; Puls, M. P. On the Core Structures of Edge Dislocations in NaCl and MgO. Consequences for the Core Configurations of Dislocation Dipoles. *Philos. Mag. A* **1989**, *59*, 821−842.
(14) Puls, M. P.; Norgett, M. J. Atomistic Calculation of the Core Structure and Peierls energy of an (a/2) [110] Edge Dislocation in MgO. *J. Appl. Phys.* **1976**, *47*, 466−477.
(15) Puls, M. P.; Woo, C. H.; Norgett, M. J. Shell-Model Calculations of Interaction Energies between Point Defects and Dislocations in Ionic Crystals. *Philos. Mag.* **1977**, *36*, 1457−1472.
(16) Puls, M. P. Vacancy−Dislocation Interaction Energies in MgO A Re-analysis. *Philos. Mag. A* **1983**, *47*, 497−513.
(17) Puls, M. P. Vacancy−Dislocation Interaction Energies in MgO. *Philos. Mag. A* **1980**, *41*, 353−368.
(18) Hoagland, R. G.; Hirth, J. P.; Gehlen, P. C. Atomic Simulation of the Dislocation Core Structure and Peierls Stress in Alkali Halide. *Philos. Mag.* **1976**, *34*, 413−439.
(19) Watson, G. W.; Kelsey, E. T.; Parker, S. C. Atomistic Simulation of Screw Dislocations in Rock Salt Structured Materials. *Philos. Mag. A* **1999**, *79*, 527−536.
(20) Walker, A. M.; Carrez, P.; Cordier, P. Atomic-Scale Models of Dislocation Cores in Minerals: Progress and Prospects. *Mineral. Mag.* **2010**, *74*, 381−413.
(21) Amelinckx, S.; Gever, R.; Van Landuyt, J. *Diffraction and Imaging Techniques in Materials Science*. 2nd ed.; North-Holland: Amsterdam, 1978.
(22) Goodhew, P. J.; Humphreys, J.; Beanlan, R. *Electron Microscopy and Analysis*. 3rd ed.; Taylor & Francis: London, 2001.
(23) Chisholm, M. F.; Pennycook, S. J. Direct Imaging of Dislocation Core Structures by Z-Contrast STEM. *Philos. Mag.* **2006**, *86*, 4699−4725.
(24) Peierls, R. E. On the Size of a Dislocation. *Proc. Phys. Soc., London* **1940**, 52−56.
(25) Nabarro, F. R. N. Dislocations in a Simple Cubic Lattice. *Proc. Phys. Soc.* **1947**, *59*, 256.
(26) Schoeck, G. The Peierls Model: Progress and Limitations. *Mater. Sci. Eng., A* **2005**, *400−401*, 7−17.
(27) Mostoller, M.; Chisholm, M. F.; Kaplan, T. New Extended Point Defect Structure in Diamond Cubic Crystals. *Phys. Rev. Lett.* **1994**, *72*, 1494−1497.
(28) Clouet, E.; Ventelon, L.; Willaime, F. Dislocation Core Energies and Core Fields from First Principles. *Phys. Rev. Lett.* **2009**, *102*, 055502−055506.
(29) Cai, W.; Bulatov, V. V.; Chang, J.; Li, J.; Yip, S. Anisotropic Elastic Interactions of a Periodic Dislocation Array. *Phys. Rev. Lett.* **2001**, *86*, 5727−5730.
(30) Clouet, E. Elastic Energy of a Straight Dislocation and Contribution from Core Tractions. *Philos. Mag.* **2009**, *89*, 1565−1584.
(31) Walker, A. M.; Gale, J. D.; Slater, B.; Wright, K. Atomic Scale Modelling of the Cores of Dislocations in Complex Materials Part 1: Methodology. *Phys. Chem. Chem. Phys.* **2005**, *7*, 3227−3234.
(32) Walker, A. M.; Gale, J. D.; Slater, B.; Wright, K. Atomic Scale Modelling of the Cores of Dislocations in Complex Materials Part 2: Applications. *Phys. Chem. Chem. Phys.* **2005**, *7*, 3235−3242.
(33) Walker, A. M.; Slater, B.; Gale, J. D.; Wright, K. Predicting the Structure of Screw Dislocations in Nanoporous Materials. *Nat. Mater.* **2004**, *3*, 715−720.
(34) Walker, A. Simulation of Screw Dislocations in Wadsleyite. *Phys. Chem. Miner.* **2010**, *37*, 301−310.
(35) Taylor, H. F. W. *Cement Chemistry*. 2nd ed.; Thomas Telford: London, 1997.
(36) Shahsavari, R.; Buehler, M. J.; Pellenq, R. J. M.; Ulm, F.-J. First-Principles Study of Elastic Constants and Interlayer Interactions of Complex Hydrated Oxides: Case Study of Tobermorite and Jennite. *J. Am. Ceram. Soc.* **2009**, *92*, 2323−2330.
(37) Ghosh, S. N. *Advances in Cement Technlogy: Chemistry, Manufacture, and Testing*. Taylor & Francis: Oxford, 2002.
(38) Mumme, W. G.; Hill, R. J.; Bushnell-Wye, G.; Segnit, E. R. Rietveld Crystal Structure Refinements, Crystal Chemistry and Calculated Powder Diffraction Data for the Polymorphs of Dicalcium Silicate and Related Phases. *Neues Jahrb. Mineral., Abh.* **1995**, *169*, 35−68.
(39) Barbier, J.; Hyde, B. G. The Structures of the Polymorphs of Dicalcium Silicate, Ca_2SiO_4. *Acta Crystallogr. Sect. B* **1985**, *41*, 383−390.
(40) Feng, X.; Min, X.; Tao, C. Study on the Structure and Characteristic of Dicalcium Silicate with Quantum Chemistry Calculations. *Cem. Concr. Res.* **1994**, *24*, 1311−1316.
(41) Smith, D. K.; Majumdar, A.; Ordway, F. The Crystal Structure of γ-Dicalcium Silicate. *Acta Crystallogr.* **1965**, *18*, 787−795.
(42) Jost, K. H.; Ziemer, B.; Seydel, R. Redetermination of the Structure of β-Dicalcium Silicate. *Acta Crystallogr., Sect. B: Struct. Crystallogr. Cryst. Chem.* **1977**, *33*, 1696−1700.
(43) Juilland, P.; Gallucci, E.; Flatt, R.; Scrivener, K. Dissolution Theory Applied to the Induction Period in Alite Hydration. *Cem. Concr. Res.* **2010**, *40*, 831−844.
(44) Hudson, K. E.; Groves, G. W. The Structure of Alite in Portland Cement Clinker—TEM Evidence. *Cem. Concr. Res.* **1982**, *12*, 61−68.
(45) Cygan, R. T.; Casey, W. H.; Boslough, M. B.; Westrich, H. R.; Carr, M. J.; Holdren, G. R., Jr. Dissolution Kinetics of Experimentally Shocked Silicate Minerals. *Chem. Geol.* **1989**, *78*, 229−244.
(46) Wang, Y. G.; Zou, B. S.; Kuo, K. H.; Feng, X. J.; Wang, L.; Long, S. Z. High-Resolution Electron Microscopy Study of Belite. *J. Mater. Sci.* **1989**, *24*, 877−880.
(47) Groves, G. W. Portland Cement Clinker Viewed by Transmission Electron Microscopy. *J. Mater. Sci.* **1981**, *16*, 1063−1070.
(48) Hewlett, P. C.; Lea, F. M. *Lea's Chemistry of Cement and Concrete*, 4th ed. Elsevier Butterworth−Heinemann: Oxford, 1998.
(49) Hirth, J. P.; Lothe, J. *Theory of Dislocations*. 2nd ed.; John Wiley & Sons: New York, 1982; p 435.
(50) Gale, J. D.; Rohl, A. L. The General Utility Lattice Program (GULP). *Mol. Simul.* **2003**, *29*, 291−341.
(51) Cygan, R. T.; Liang, J.-J.; Kalinichev, A. G. Molecular Models of Hydroxide, Oxyhydroxide, and Clay Phases and the Development of a General Force Field. *J. Phys. Chem. B* **2004**, *108*, 1255−1266.
(52) Kirkpatrick, R. J.; Kalinichev, A. G.; Wang, J. Molecular Dynamics Modelling of Hydrated Mineral Interlayers and Surfaces: Structure and Dynamics. *Mineral. Mag.* **2005**, *69*, 289−308.
(53) Kirkpatrick, R. J.; Kalinichev, A.; Jianwei, W. Molecular Modeling of Confined Fluids and Solid−Fluid Interfaces in Portland Cement and Related Materials. In *NanoTechnology in Construction*; Bartos, P., Ed. The Royal Society of Chemistry United Kingdom: Cambridge, United Kingdom, 2004.
(54) Hill, R. The Elastic Behaviour of a Crystalline Aggregate. *Proc. Phys. Soc., Sect. A* **1952**, *65*, 349.

DOI: 10.1021/am5091808
ACS Appl. Mater. Interfaces 2015, 7, 2223−2234

(55) Puls, M. P.; Horgett, M. J. Atomistic Calculation of the Core Structure and Peierls Energy of an (a/2) [110] Edge Dislocation in MgO. *J. Appl. Phys.* **1976**, *47*, 466.
(56) Vítek, V.; Perrin, R. C.; Bowen, D. K. The Core Structure of 1/2(111) Screw Dislocations in bcc Crystals. *Philos. Mag.* **1970**, *21*, 1049−1073.
(57) Xu, G.; Argon, A. S. Energetics of Homogeneous Nucleation of Dislocation Loops under a Simple Shear Stress in Perfect Crystals. *Mater. Sci. Eng., A* **2001**, *319−321*, 144−147.
(58) Denoual, C. Modeling Dislocation by Coupling Peierls−Nabarro and Element-free Galerkin Methods. *Comput. Methods. Appl. Mech. Eng.* **2007**, *196*, 1915−1923.
(59) Blumenau, A. T.; Heggie, M. I.; Fall, C. J.; Jones, R.; Frauenheim, T. Dislocations in Diamond: Core Structures and Energies. *Phys. Rev. B* **2002**, *65*, 205205.
(60) Han, S. M.; Feng, G.; Jung, J. Y.; Jung, H. J.; Groves, J. R.; Nix, W. D.; Cui, Y. Critical-Temperature/Peierls-Stress Dependent Size Effects in Body Centered Cubic Nanopillars. *Appl. Phys. Lett.* **2013**, 102.
(61) Young, J. F. Highly Reactive Dicalcium Silicates for Belite Cement. In *From Material to Structure*, Proceeding of the International RILEM Conference on Concrete. Bournazel, J.-P., Malier, Y., Eds.; RILEM Publications: Bagneux, France, 1988, pp 1−15.
(62) Watson, G. W.; Oliver, P. M.; Parker, S. C. Atomistic Simulation of Crystal Growth at the ⟨100⟩ Screw Dislocation Terminating at the {100} Surface of MgO. *Surf. Sci.* **2001**, *474*, L185−L190.
(63) Shahsavari, R.; Pellenq, R.; Ulm, F.-J. Empirical Force Fields For Complex Calcio-Silicate Layered Materials. *Phys. Chem. Chem. Phys.* **2011**, *13*, 1002−1011.
(64) Sakhavand, N.; Muthuramalingam, P.; Shahsavari, R. Toughness Governs the Rupture of Interfacial H-Bond Assemblies at a Critical Length Scale in Hybrid Materials. *Langmuir* **2013**, *29*, 8154−163.
(65) Jalilvand, S.; Shahsavari, R. Molecular Mechanistic Origin of Nanoscale Contact, Friction and Scratch in Complex Particulate Systems, *ACS Appl. Mater. Interfaces*. DOI:10.1021/am506411h.
(66) Pellenq, R. J. M.; Kushima, A.; Shahsavari, R.; Vliet, K. J. V.; Buehler, M. J.; Yip, S.; Ulm, F. J. A Realistic Molecular Model of Cement Hydrates. *Proc. Natl. Acad. Sci. U.S.A.* **2009**, *106*, 16102−16107.
(67) Abdolhosseini Qomi, M. J.; Krakowiak, K. J.; Bauchy, M.; Stewart, K. L.; Shahsavari, R.; Jagannathan, D.; Brommer, D. B.; Baronnet, A.; Buehler, M. J.; Yip, S.; Ulm, F.-J.; Pellenq, R. Combinatorial Molecular Optimization of Cement Hydrates. *Nat. Commun.* **2014**, *5*, 4960.
(68) Shahsavari, R. Hierarchcial Modeling of Structure and Mechanics of Cement Hydrates. Ph.D. Thesis, Massachusetts Institute of Technology, Cambridge, MA, 2011.
(69) Rafiee, M. A.; Narayanan, T. N.; Hashim, D. P.; Sakhavand, N.; Shahsavari, R.; Vajtai, R.; Ajayan, P. M. Hexagonal Boron Nitride and Graphite Oxide Reinforced Multifunctional Porous Cement Composites. *Adv. Funct. Mater.* **2013**, *23*, 5624−5630.
(70) Muthuramalingam, P.; Sakhavand, N.; Shahsavari, R. H_2, N_2, and CH_4 Gas Adsorptions in Zeolitic Imidazolate Framework-95 and -100: Ab Initio Based Grand Canonical Monte Carlo Simulation. *J. Phys. Chem. C* **2013**, *117*, 24407−24416.

NOTE ADDED AFTER ASAP PUBLICATION

This paper was published on the Web on January 20, 2015. Additional information was added to the Acknowledgment section, and the paper was reposted on January 21, 2015.

DOI: 10.1021/am5091808
ACS Appl. Mater. Interfaces 2015, 7, 2223−2234